City Research Online

City, University of London Institutional Repository

This is the accepted version of the paper.

This version of the publication may differ from the final published version.

Synchrotron radiography studies of shear-induced dilation in semi-solid Al alloys and steels

C.M. Gourlay[1], C. O'Sullivan[2], J. Fonseca[3], L. Yuan[4], K.M. Kareh[1], T. Nagira[5], and H. Yasuda[6]

1.—Department of Materials, Imperial College, London SW7 2AZ, UK.
2.—Department of Civil and Environmental Engineering, Imperial College, London SW7 2AZ, UK.
3.—Department of Civil Engineering, City University, London EC1V 0HB, UK.
4.—GE Global Research, Niskayuna, NY 12309, USA.
5.—Department of Adaptive Machine Systems, Osaka University, Suita, Osaka 565-0871, Japan.
6.—Department of Materials Science and Engineering, Kyoto University, Sakyo-ku, Kyoto 606-8501, Japan.

Abstract

An improved understanding of the response of solidifying microstructures to load is required to further minimize casting defects and optimize casting processes. This article overviews synchrotron radiography studies that directly measure the micromechanics of semisolid alloy deformation in a thin sample direct-shear cell. It is shown that shear-induced dilation (also known as Reynolds' dilatancy) occurs in semisolid alloys with morphologies ranging from equiaxed-dendritic to globular, at solid fractions from the dendrite coherency point to ~90% solid, and it occurs in both Al alloys and carbon steels. Discrete-element method simulations that treat solidifying microstructures as granular materials are then used to explore the origins of dilatancy in semisolid alloys.

1   Introduction

Many casting defects have their origin in the natural flow, shrinkage/contraction and gas evolution that occurs during solidification. Additionally, it is common for a casting process to deform the solidifying alloy, either intentionally such as the application of pressure in high-pressure die casting and squeeze casting, or unintentionally such as the deformation of bulges between rolls in continuous casting. Therefore, in order to minimise casting defects and optimise casting processes, we require a detailed understanding of how solidifying microstructures respond to load and how deformation leads to casting defects.

Despite this importance, the study of semi-solid alloy deformation has received little attention compared with fully-solid alloys and our understanding is much less developed. The focus of a large proportion of past work has been on either low solid fraction suspension rheology relevant to semi-solid processing routes such as rheocasting (*1-3*), or on tensile loading at high solid fraction (>~0.90) relevant to hot tearing (*4-6*), and there are combinations of semi-solid microstructure and loading mode that remain largely unexplored.

A common mode of solidification in casting is the nucleation and growth of numerous equiaxed crystals. In the case that no other phase forms first, free crystals impinge on one another during growth, creating a crystal network (*1*). This point is commonly termed "dendrite coherency" (*7-9*), although this term is also used to describe other transitions in the mushy zone (*10*). Dendrite coherency marks the onset of measurable shear and compressive strength but the alloy has negligible tensile strength at this stage as there is negligible cohesion between crystals (*1, 11*). Recently, it has been found that shear/compressive deformation at solid fractions above dendrite coherency causes shear-induced dilation (*12*) (also known as Reynolds' dilatancy (*13*)). This is the phenomenon in granular materials whereby the volume occupied by the particles/grains increases during shear (i.e. the packing density of the particles decreases during shear). This occurs when the particles are sufficiently compacted that they push or lever one another apart as they begin to rearrange under load. Shear-induced dilation is a fundamental mechanical property of granular materials such as dense particulate soils (*14*) and powders but was not expected of partially-solid alloys.

Subsequent studies have shown that dendrite coherency marks the onset of dilatancy (i.e. shear-induced dilation) in partially-solid alloys (*12, 15, 16*), and it has been suggested that dilatancy may be important in semi-solid processing (*17*), high-pressure die casting (*18*), and direct chill casting (*19*). However, this remains a little explored area and the development of physically-based models that

include shear-induced dilation requires an improved understanding of the fundamentals. Therefore, the aims of this work have been: (i) to obtain direct proof of shear-induced dilation in semi-solid alloys, (ii) to understand the micromechanics of semi-solid deformation at intermediate solid fraction and how they lead to shear-induced dilation, and (iii) to explore modelling techniques that are well-suited to capturing shear-induced dilation in semi-solid alloys.

2   Methods

Time-resolved synchrotron radiography experiments were performed in a thin-sample direct-shear cell shown in Figure 1, which is loosely based on the shear-box test in soil mechanics (e.g. (20)). The rig was developed to study assemblies of numerous equiaxed crystals that are approximately one crystal thick. All semi-solid deformation experiments were conducted isothermally on partially-remelted samples. A variety of semi-solid grain morphologies were created by altering the prior solidification and coarsening treatments. An equiaxed-dendritic morphology was generated by partially remelting an equiaxed-dendritic cast microstructure and isothermally holding for 20 min prior to deformation. Globular morphologies were generated by applying a ~1 week semi-solid heat treatment prior to partial-remelting, thermal equilibration and deformation. All experiments reported here involved combinations of solid fraction and crystal morphology that resulted in an assembly of crystals in mechanical contact.
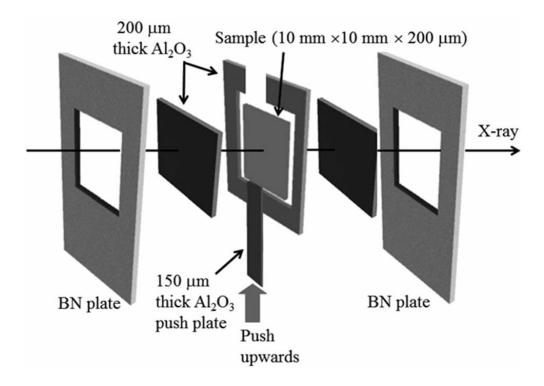

Figure 1. Schematic of the thin-sample shear cell used for synchrotron radiography experiments on Al-Cu samples. N.B. samples were 180 μm thick in experiments on steels.

The rig was incorporated into beamline BL20B2 at the SPring-8 synchrotron in Hyogo, Japan (*21*). The displacement rate was set to du_z/dt = 100 μm s^{-1}, giving a global shear rate of ~1x10^{-2} s^{-1}. Deformation was conducted to accumulated global shear strains of γ~10–30%. Some experiments were conducted on Al-15Cu alloys which have strong solid–liquid contrast in the transmitted X-ray images. Other experiments were conducted on Fe-2C alloys to develop the deformation/imaging technique towards industrially relevant steels. The challenges of imaging solidification phenomena in carbon steels are overviewed in ref (*22*). Full experimental details on imaging and deformation can be found in ref. (*23*) for Al-Cu alloys and ref. (*24*) for Fe-C alloys.

3   Results and Discussion

3.1   General Phenomena

The phenomenon of shear-induced dilation is summarised in Figures 2(a)-(b) for the simplified case of ordered packings of circles in homogeneous compressive loading modes. The Figure depicts quasi-rigid grains with negligible inter-grain cohesion where force is transmitted across grain-grain contacts and the resulting macroscopic shape change occurs by grain rearrangement. This behaviour is often termed granular deformation and materials that exhibit this behaviour are often termed packed granular materials (*25*). It can be seen that, under these conditions, geometry dictates that the application of a shear strain generates volumetric strain, accommodated by an increase in the volume of interstitial spaces. Note that it is common to define strain with respect to the solid assembly rather than the whole material, so that a decreasing packing-density of the grains is defined as a dilatational volumetric strain (*14*). For the case of homogeneous shear of uniform circles from the close packed to least packed configuration (from a hexagonal array to square array), the volumetric strain is a ~15.5% dilation $\left(\frac{2}{\sqrt{3}} - 1\right)$. Note that the continued shear of Fig. 2b would lead to the grains being pushed closer together again (a contractive volumetric strain), and to cyclic dilation and contraction. This is a feature of the ordered packing of monodisperse circles. In disordered polydisperse packings found in nature (e.g., soils, powders, etc.), there are local regions of compaction and dilation, and the overall volumetric strain comes from a combination of local dilation and compaction that is either net-contractive, net-dilational, or constant volume deformation.

It might be thought that partially-solid alloys containing a solid network would not deform in this way because the grains have a yield strength of only up to a few MPa at T/T_m~1 (*26, 27*) and grain-grain contacts can be cohesive due to the formation of solid-solid interfaces where the

4

misorientation angle is favourable (*28, 29*). However, direct in-situ imaging has shown that semi-solid alloys often deform by shear-induced dilation (*23, 24, 30, 31*). As an example, Figure 2(c) shows a local region of microstructure where the configuration of four grains and the loading direction are similar to the geometry in Figure 2(a). In Figure 2(c) it can be directly observed that, during loading, the grains push each other apart in a manner similar to Figure 2(a). It can also be seen that the expansion of interstitial spaces is compensated by the in-flow of liquid (dark) from elsewhere in the sample.
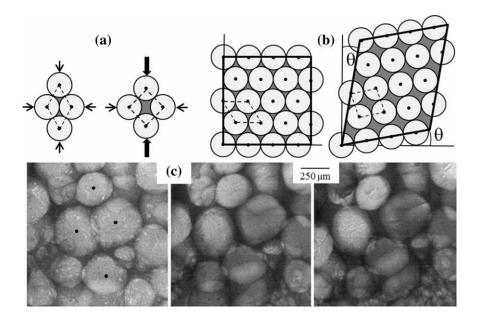

Figure 2. (a, b) Shear-induced dilation of ordered close-packed circles: (a) four circles in biaxial compression and (b) 20 circles in pure shear. Grains are light gray, grain centroids are marked with dots, interstitial liquid is shaded dark grey and arrows indicate the direction and magnitude of force. (c) Four globules in Al-15Cu at ~70% solid (centroids marked with dots) loaded similar to (a).

In general, partially-solid alloy microstructures that develop during equiaxed solidification are disordered packings of polydisperse grains with complex shapes and complex contacts. Therefore, in-situ studies were performed on semi-solid alloys of a variety of solid fractions and crystal morphologies to study the micromechanics in a range of semi-solid alloys (*23, 30, 31*). These studies have found that, during loading in the shear-cell, the microstructural response to load shares common features whenever the partially-solid alloy consists of numerous equiaxed grains in mechanical contact and there is sufficient interstitial liquid to feed volumetric strains. These common features are: (i) there is rarely any discernible deformation of the individual grains, (see section 3.4 for an exception to this statement), (ii) macroscopic shape change occurs predominantly by grain rearrangement coupled with interstitial liquid flow; (iii) most grains translate and rotate as discrete bodies under the action of contact forces; (iv) rearrangement causes the local grain packing-density (the local solid fraction) to adjust under load with a combination of local compaction and

local dilation. For the combinations of solid fraction, morphology and strain rate overviewed in this paper, changes in solid fraction were accommodated by the in-flow or out-flow of the interstitial liquid from other regions of the samples; (v) macroscopic shear-induced dilation occurs causing the overall solid fraction to decrease during grain rearrangement, and (iv) grain motion often becomes localized in certain areas, producing inhomogeneous deformation.

We next focus on the detailed grain-scale response to load in three datasets from microstructures containing numerous equiaxed grains in mechanical contact but which have markedly different semi-solid microstructures: equiaxed-dendritic at 30% solid, globular at ~70% solid and globular-polygonal at ~88% solid.

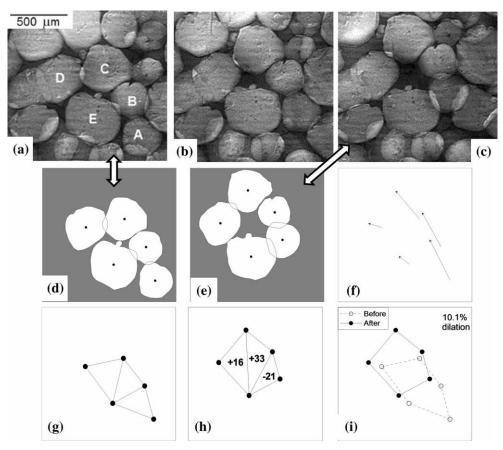Figure 3. Local region of shear-induced dilation in globular Al-15Cu. (a–c): Radiographs of globules pushing each other apart during rearrangement. (d and e): Projected-area globule outlines and centroids. (f) Centroid displacements from (d) to (e). (g and h): Triangulation of the globule centroids. The values in (h) are the % volumetric strain of the triangles. (i) Overall area change of the centroid polygons = 10.1% dilation.

3.2   Globular Al-15Cu at ~70% solid

Figures 3 and 4 overview results from a globular Al-15Cu sample deformed at ~70% solid (produced by an 8-day semi-solid heat treatment to globularise the αAl prior to the experiment). It can be seen that the initial microstructure is a disordered assembly of grains in mechanical contact with liquid filling the interstitial spaces. The sample thickness is ~0.6 median grain diameters, producing a near-monolayer of grains that have been sectioned into 'disks' during sample preparation, and there is some overlap between the grains in the projected-area images. During loading in the shear-cell there are regions of local compaction and local dilation.

An example of local dilation is overviewed in Figure 3, which is a region near the half-plane of the shear-cell. Note that the pushing-plate is below-right of the grain labelled A in Figure 3(a). As the plate moves upwards, grain A pushes B and C up and to the left, and A,B and C slide past D and E between Figures 3(a) and (b). Now A is in contact with both B and E and, as A is pushed further up-left, the position of the contacts between A-B and A-E causes grain A to push B and E apart (compare Figures 3(b) and (c)). These grain movements are due to force transmission across contacts, and cause the packing-density of the grains to decrease and the volume of liquid-filled spaces to increase. The projected grain perimeters and centroids corresponding to (a) and (c) are plotted in Figures 3 (d)-(e) respectively. The centroid displacement field contains diverging vectors in Figure 3 (f) since grains are pushing each other apart. In Figures 3 (g)-(i), the local dilatational volumetric strain is quantified by triangulation of the centroids in Figures 3 (d) and (e).   The values in each triangle show the volumetric strain in each triangle, and the overall dilation of this local assembly is 10.1 % as shown in Figure 3(i).

Figure 4. Deformation of globular Al-15Cu at ~70% solid, highlighting the role of the rotation of an agglomerate of grains C and F with bowling pin shape. White dots mark the contacts important in causing rotation, white lines are the primary axis of the agglomerate formed by grains C and F, and the dashed line is the circle with diameter equal to the primary axis of the agglomerate. The push plate can be seen to the far right of each image.

Figure 4 is the same region as that in Figure 3 but spanning a longer period of deformation. In Figure 4, it can be inferred from the motion of grain C that this grain is actually welded to (has a solid-solid interface with) the grain to its right, making an effective structural unit shaped like a 'bowling pin'. In Figure 3, grain C only translates upwards, but in Figure 4 grain C undergoes significant rotation. This is because non-spherical particles have both normal and tangential components of contact force that induce a moment on grains, and the position of the two contacts marked with white dots in Figure 4 and noting that the contact normal force is not collinear with the vector joining the centroids (the branch vector), causing the contact normal force to apply a significant moment. Between Figure 4(b) and (c), the major axis of grain C undergoes a 46° anticlockwise rotation which creates significant interstitial space because a 'bowling pin' shape sweeps-out a much larger projected-area than its true projected-area. Therefore, the rotation of grain C with high aspect ratio causes strong local dilation.
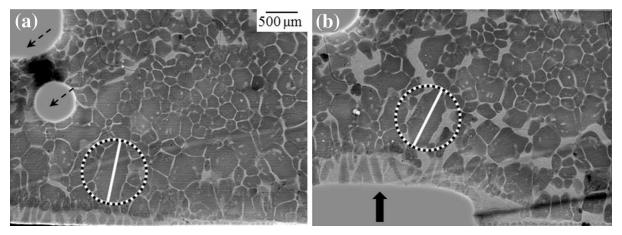

Figure 5. Deformation of globular–polygonal Fe-2C-1Mn-0.5Si at ~88% solid: (a) prior to deformation and (b) after 1072 μm (3.1 mean grains) of push-plate displacement. Note the significantly enlarged liquid-filled interstices in (b) due to shear-induced dilation. The primary axis and circle of rotation are shown for a large grain with high aspect ratio. Austenite is dark gray, liquid is light gray, and the rounded features marked with arrows are pores.

3.3   Globular-polygonal Fe-2C-1Mn-0.5Si at ~88% solid

Figure 5 shows images of the entire field of view at two stages during the deformation of a semi-solid high-carbon steel at ~88% solid. This sample was produced by an extended semi-solid heat treatment of 100 h at ~70% solid under Ar (*31*). The combination of the high solid fraction and semi-solid coarsening treatment has created a grain morphology that is partially globular and partially polygonal, with some solid–liquid interfaces that are concave to accommodate the convex solid–liquid interfaces of neighbouring grains and with many interfaces that are relatively straight. Note that austenite grains are dark and the liquid bright in Figure 5 (the opposite to the Al-Cu radiographs).It can be seen in Figure 5 that deformation at such high solid fraction leads to strong shear-induced dilation with large liquid-filled spaces opening up between grains during shear. As

8

discussed in reference (*30*), this liquid was drawn in from the sides of this sample and there was no measurable deformation of the individual grains at the resolution of the experiment.

Similar to the globular sample at 70% solid in Figures 3 and 4, shear-induced dilation in Figure 5 is caused by the translation and rotation of quasi-rigid grains that were initially tightly packed. The rotation of a large grain with relatively high aspect ratio is highlighted in Figure 5. This grain rotates 14° clockwise between the two frames in Figure 5, which levers neighbouring grains apart and creates significant interstitial space.
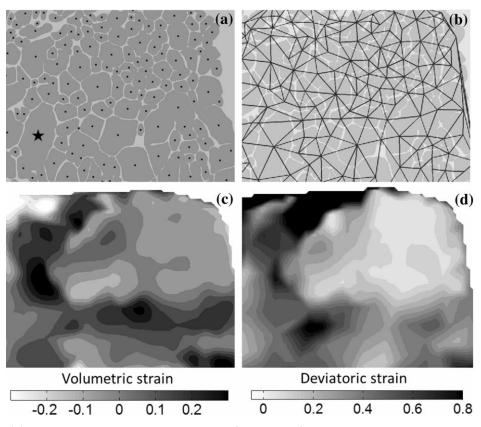

Figure 6. (a) Separated grains and their centroids from part of Fig 5a. The centroid marked with a star is the grain highlighted in Figure 5. (b) Delaunay triangulation of the centroids. (c) Volumetric strain field where positive values indicate dilation. (d) Deviatoric strain field. The strain fields have been smoothed and are for the deformation increment from Figure 5(a) and (b).

The inhomogeneous strain field can be quantified from these experiments by first segmenting the grains and triangulating the grain centroids. Then the strain in each triangle, defined by a triad of three centroids, can be calculated from the centroid displacements using the constant strain triangle shape functions from finite-element analysis (e.g. (*32*)) in a way similar to Figure 3h. This has been performed for a portion of the steel dataset from Figure 5 and the results are shown in Figure 6. Figure 6(a) is a plot of the segmented and separated grains and their centroids in the undeformed state. Figure 6(b) is a Delaunay triangulation of the initial centroids and Figures 6(c) and (d) are the

volumetric and deviatoric strain fields respectively for the deformation increment shown in Figure 5. The strain fields have been smoothed to aid visualization because there are large variations in strain from triangle to triangle (as can be seen for volumetric strain in Figure 3(h). Note that there are local regions of positive and negative volumetric strain, and the overall behavior is net-dilatational. In Figure 6(d), the shear strains are taken as the difference between the eigenvalues of the strain tensor in each triangle.

Figures 6(c) and (d) quantify the inhomogeneous volumetric and shear strain fields. It can be seen that, in general, regions of high shear correspond to regions of high dilation. A region of high shear and simultaneous dilation has developed both in a vertical band and a horizontal band that start close to the large grain highlighted in Figure 5. As shown in reference (*31*), the regions of high shear and dilatational volumetric strain in this sample correspond to regions of highest grain rotation, the greatest reduction in number of contacts per grain, and the greatest increase in distance between neighboring grains.

3.4 *Equiaxed-dendritic Al-15Cu at ~30% solid*

Since macroscopic rheology experiments have measured that the dendrite coherency point marks the onset of dilatancy in equiaxed solidification (*12, 15, 16*), in-situ experiments were conducted on equiaxed-dendritic microstructures slightly above the dendrite coherency point. Figure 7(a) shows Al-15Cu at ~30% solid with an equiaxed-dendritic morphology, produced by partially remelting a coarse equiaxed-dendritic cast microstructure and isothermally holding for 20 min prior to deformation (*23*). This combination of crystal morphology and low solid fraction results in an assembly of crystals in contact because a significant proportion of the liquid is within dendrite envelopes and the envelopes are in mechanical contact. Note that, for equiaxed solidification in general, while the dendrite coherency solid fraction can vary from ~0.15–0.5(*7, 8*), the envelope fraction at coherency has been shown to fall within a much higher and narrower range of 0.56–0.70 (*33*).
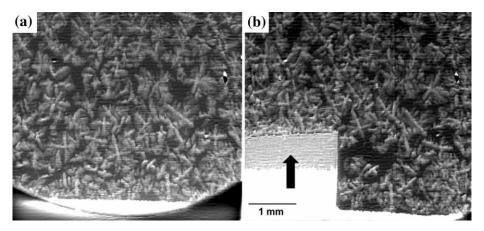
Figure 7. Radiographs of Al-15Cu with equiaxed-dendritic morphology at ~30% solid: (a) prior to deformation and (b) after 1606 μm (3.8 mean grains) of push-plate displacement.

Comparing Figures 7(a) and (b), it can be seen that, in most of the field of view, deformation was accommodated by grain rearrangement by discrete translations and rotations of the crystal envelopes. The exception to this occurred at the pushing-plate front where global deformation occurred by crystal deformation and the crystal assembly deformed as a viscoplastic solid skeleton that squeezed out interstitial liquid as it was compressed. This shows that there is added complexity in equiaxed-dendritic structures caused by a competition between deformation of the individual grains and rearrangement of grains that was not measured for the globular and globular-polygonal structures in sections 3.2 and 3.3.

Away from the small region at the leading edge of the pushing-plate where the individual grains were deformed, shape change was by rearrangement of the envelopes. Dendritic grain rearrangement caused local compaction and local dilation. An example of local dilation is shown in Figure 8 involving 12 crystals labelled A-L. In Figures 8(a) and (b), the liquid-filled space between the 11 envelopes dilates due to the dendritic grains pushing and levering each other apart similar to the globular grains in Figure 3. Note that the pushing-plate displacement between Figure 8a and b is ~0.2 d_{50}-(where d_{50} is the median projected grain size). Of particular importance in this dilation event is the small clockwise rotation of grain G which pushes grain H upwards and grain I down and right, creating interstitial space. The projected grain perimeters and centroids corresponding to Figures 8(a) and (b) are plotted in Figure 8 (c)-(d) respectively. The centroid displacement field in Figure 8(e) shows that the grains are moving to the right, away from the advancing pushing-plate and that there is a slight divergence to the vectors. In Figures 8(f)-(g), the local dilatational volumetric strain is quantified by triangulation of the centroids in Figures 8(c) and (d). The values in each triangle show the volumetric strain in each triangle, and the overall dilation of this local assembly is 1.9 % as shown in Figure 8(h).
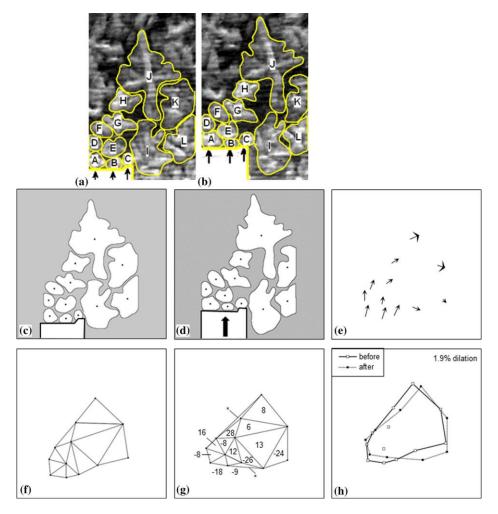
11

Figure 8. Local region of shear-induced dilation in equiaxed-dendritic Al-15Cu at _30% solid. (a, b): Radiographs of 12 crystals with envelopes estimated in yellow. (c and d): Projected-area envelope outlines and centroids. (e) Centroid displacements from (c) to (d). (f and g): Triangulation of the globule centroids. The values in (g) are the % volumetric strain of the triangles. (i) Overall area change of the centroid polygons = 1.9% dilation.

Comparing the deformation of the equiaxed-dendritic microstructure inFigures 7 and 8 with the globular microstructure in Figures 3 and 4 and the globular-polygonal microstructure in Figures 5 and 6, there are a variety of differences in the details of the micromechanics. For example, the contacts across which force is transmitted in the equiaxed-dendritic and globular microstructures are relatively well-approximated as point contacts similar to the circles in Figures 2(a) and (b). In contrast, a high proportion of each grain perimeter is involved in force transmission in the globular-polygonal microstructure in Figures 5 and 6. Additionally, the magnitude of the shear-induced dilation is significantly different in each microstructure which is mostly due to the different initial packing-densities of the crystal envelopes. Despite these differences, each microstructure deforms predominantly by grain rearrangement and undergoes shear-induced dilation, highlighting the ubiquity of this phenomenon in equiaxed semi-solid microstructures containing a solid network.

3.5   Discrete Element Method (DEM) modelling

The synchrotron radiography studies have shown that, during deformation of semi-solid alloys containing a solid network in the thin-sample shear-cell in Figure 1, shape change predominantly occurs by the rearrangement of grains within an assembly of grains in mechanical contact, and that shear-induced dilation is a fundamental part of the microstructural response to load.   Other materials that exhibit these deformation phenomena such as soils (*34*), powders and other compacted granular materials are often modelled using the particulate discrete element method (DEM). In DEM, the material is explicitly treated as an assembly of particles that can move independently by translation and rotation caused by forces acting at particle–particle contacts (*35*), and shear-induced dilation emerges naturally with this approach.

A DEM model was developed within the commercial DEM package PFC[2D] (Itasca Consulting Group, Inc. based on ref. (*35*)) that takes simulated 2D solidification microstructures as inputs and models the microstructural response to an imposed deformation (*33*).   The study in reference (*33*) used equiaxed solidification microstructures modelled with the approach of Lee and co-workers (*36*) and showed that dendrite coherency can be considered to be the lowest solid fraction at which long-range interconnectivity in the force chain network develops during shear and confirmed that dendrite coherency marks the lowest solid fraction at which shear-induced dilation occurs.   The study can also be used to gain insights on shear-induced dilation in a grain assembly created by equiaxed solidification.
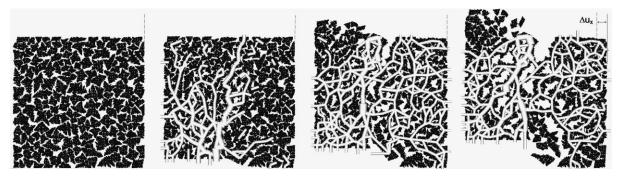

Figure 9. Two-dimensional DEM simulation of shear-induced dilation in an equiaxed-dendritic microstructure deformed in direct shear. The left hand side wall is stationary and a constant stress condition has been applied to the right-hand side wall such that it adjusts its horizontal displacement to maintain a constant stress. Dashed black lines are the initial right-hand wall position and solid black lines are the current position. The white lines are force chains with line thickness proportional to force magnitude. Force is transmitted across crystal–crystal contacts and shear-induced dilation Δu_z emerges naturally from the simulation. Full details are given in Ref. 33.

Figure 9 shows a simulated 2D equiaxed-dendritic microstructure that was deduced to be above the dendrite coherency solid fraction in ref. (*33*).   The Figure shows a DEM simulation of this

microstructure during loading in direct-shear with some similarities to the thin-sample shear cell in Figure 1. In this DEM simulation, the left-hand side wall is defined as stationary and a constant stress condition has been applied to the right-hand side wall such that, if the stress acting on the right-hand wall reaches a critical value the right-hand wall adjusts its horizontal displacement and a constant stress is maintained by a servo-mechanism. Full details are given in reference (*33*). White lines are force chains and the line thickness is proportional to force magnitude. It can be seen that, as the pushing-plate begins to move upwards, grain–grain contacts are created through which force can be transmitted and force chains develop vertically. With continued pushing-plate displacement, the force chain network develops throughout most of the sample and force is transmitted to the right-hand side wall. With further pushing-plate displacement, there comes a point when the critical stress on the right-hand wall is exceeded and the right hand wall moves to the right, leading to a dilatational volumetric strain. This can be seen by noting that dashed black lines are the initial right-hand wall position and solid black lines are the current position. In this way, shear-induced dilation emerges naturally from the simulation. It is also of interest to note that, if the crystal assembly is constrained to rearrange at constant volume and the grains are defined to be rigid, this microstructure becomes jammed (as shown in Figures 4(c),(f) and (i) in ref. (*33*)). Thus, we would expect the mechanical response to be pressure sensitive and, additionally, the competition between grain rearrangement and the deformation of individual grains to be pressure sensitive.

Particulate numerical modelling including the DEM has been applied to semi-solid alloy deformation by other groups (*37-39*) which are combining finite element and discrete element methods to account for the viscoplastic deformation of the solid. The in-situ imaging results and these initial models suggest that DEM is likely to be an important component within future models of mush mechanics.

4   Summary

In-situ studies of semi-solid deformation have provided direct proof for shear-induced dilation in semi-solid alloys with morphologies ranging from equiaxed-dendritic to globular and solid fractions ranging from dendrite coherency to ~90% solid. It has been shown that this behaviour is due to load transmission across grain-grain contacts and grains rearranging as largely-cohesionless, quasi-rigid bodies within a network of grains in mechanical contact. It has been shown that these deformation characteristics can be captured by the discrete element method (DEM) which has significant potential as a component of mush mechanics models.

5   Acknowledgements

References

1.   M. C. Flemings, Behavior of Metal Alloys in the Semisolid State. *Metallurgical Transactions A* **22**, 957 (1991).
2.   H. V. Atkinson, Modelling the semisolid processing of metallic alloys. *Progress in Materials Science* **50**, 341 (2005).
3.   S. Zabler *et al.*, Particle and liquid motion in semi-solid aluminium alloys: A quantitative in situ microradioscopy study. *Acta Materialia* **61**, 1244 (2013).
4.   M. M'Hamdi, A. Mo, C. L. Martin, Two-phase modeling directed toward hot tearing formation in aluminum direct chill casting. *Metallurgical and Materials Transactions A* **33**, 2081 (Jul, 2002).
5.   S. Terzi *et al.*, In situ X-ray tomography observation of inhomogeneous deformation in semi-solid aluminium alloys. *Scr. Mater.* **61**, 449 (Sep, 2009).
6.   D. G. Eskin, Suyitno, L. Katgerman, Mechanical properties in the semi-solid state and hot tearing of aluminium alloys. *Progress in Materials Science* **49**, 629 (2004).
7.   L. Arnberg, G. Chai, L. Bäckerud, Determination of Dendritic Coherency in Solidifying Melts by Rheological Measurements. *Materials Science and Engineering A* **173**, 101 (Dec 20, 1993).
8.   N. L. M. Veldman, A. K. Dahle, D. H. StJohn, L. Arnberg, Dendrite Coherency of Al-Si-Cu Alloys. *Metallurgical and Materials Transactions A* **32A**, 147 (2001, 2001).
9.   A. K. Dahle, L. Arnberg, Development of strength in solidifying aluminium alloys. *Acta Materialia* **45**, 547 (1997, 1997).
10.   J. A. Dantzig, M. Rappaz, *Solidification*. (EPFL Press, 2009).
11.   A. K. Dahle, S. Instone, T. Sumitomo, Relationship between tensile and shear strengths of the mushy zone in solidifying aluminum alloys. *Metallurgical and Materials Transactions A* **34**, 105 (Jan, 2003).
12.   C. M. Gourlay, A. K. Dahle, Dilatant shear bands in solidifying metals. *Nature* **445**, 70 (2007).
13.   O. Reynolds, On the dilatancy of media composed of rigid particles in contact. *Philosphical Magazine* **20**, 469 (1885).
14.   A. Schofield, C. Wroth, *Critical State Soil Mechanics*. (McGraw-Hill, 1968).
15.   C. M. Gourlay, B. Meylan, A. K. Dahle, Shear mechanisms at 0-50% solid during equiaxed dendritic solidification of an AZ91 magnesium alloy. *Acta Materialia* **56**, 3403 (2008).
16.   B. Meylan, S. Terzi, C. M. Gourlay, A. K. Dahle, Dilatancy and rheology at 0-60% solid during equiaxed solidification. *Acta Materialia* **59**, 3091 (May, 2011).
17.   F. Pineau, G. Simard, Investigation of the primary phase segregation during the filling of an industrial mold with semi-solid A357 aluminum. *Solid State Phenomena* **141-143**, 635 (2008).
18.   C. M. Gourlay, H. I. Laukli, A. K. Dahle, Defect band characteristics in Mg-Al and Al-Si high pressure die castings. *Metallurgical and Materials Transactions A* **38**, 1833 (2007).
19.   T. Carlberg, A. E. W. Jarfors, On Vertical Drag Defects Formation During Direct Chill (DC) Casting of Aluminum Billets. *Metallurgical and Materials Transactions B-Process Metallurgy and Materials Processing Science* **45**, 175 (Feb, 2014).
20.   W. Powrie, *Soil Mechanics: concepts and applications*. (Spon Press, Oxford, ed. 2nd, 2002).
21.   S. Goto *et al.*, Construction and commissioning of a 215-m-long beamline at SPring-8. *Nuclear Instruments & Methods in Physics Research A* **467**, 682 (2001).

22. H. Yasuda *et al.*, Development of X-ray Imaging for Observing Solidification of Carbon Steels. *ISIJ International* **51**, 402 (2011).

23. C. M. Gourlay *et al.*, Granular deformation mechanisms in semi-solid alloys. *Acta Materialia* **59**, 4933 (2011).

24. T. Nagira *et al.*, Characterization of Shear Deformation Based on In-situ Observation of Deformation in Semi-solid Al-Cu Alloys and Water-particle Mixture. *ISIJ International* **53**, 1195 (2013).

25. H. M. Jaeger, S. R. Nagel, Physics of the granular state. *Science* **255**, 1523 (1992).

26. J. Pilling, A. Hellawell, Mechanical Deformation of Dendrites by Fluid Flow. *Metallurgical and Materials Transactions* **27A**, 229 (1996).

27. D. Fuloria, P. D. Lee, An X-ray microtomographic and finite element modeling approach for the prediction of semi-solid deformation behaviour in Al-Cu alloys. *Acta Materialia* **57**, 5554 (Oct, 2009).

28. M. Rappaz, A. Jacot, W. J. Boettinger, Last-Stage Solidification of Alloys: Theoretical Model of Dendrite-Arm and Grain Coalescence. *Metallurgical and Materials Transactions A* **34**, 467 (2003).

29. O. Ludwig, J. M. Drezet, C. L. Martin, M. Suéry, Rheological behavior of Al-Cu alloys during solidification: Constitutive modeling, experimental identification, and numerical study. *Metallurgical and Materials Transactions A* **36A**, 1525 (Jun, 2005).

30. T. Nagira *et al.*, Direct observation of deformation in semi-solid carbon steel. *Scr. Mater.* **64**, 1129 (Jun, 2011).

31. J. Fonseca, C. O'Sullivan, T. Nagira, H. Yasuda, C. M. Gourlay, In situ study of granular micromechanics in semi-solid carbon steels. *Acta Materialia* **61**, 4169 (Jun, 2013).

32. C. O'Sullivan, J. D. Bray, S. F. Li, A new approach for calculating strain for particulate media. *International Journal for Numerical and Analytical Methods in Geomechanics* **27**, 859 (2003).

33. L. Yuan, C. O'Sullivan, C. M. Gourlay, Exploring dendrite coherency with the discrete element method. *Acta Materialia* **60**, 1334 (Feb, 2012).

34. C. O' Sullivan, *Particulate Discrete Element Modelling: A Geomechanics Perspective* (Taylor & Francis 2011).

35. P. A. Cundall, O. D. L. Strack, Discrete numerical model for granular assemblies. *Geotechnique* **29**, 47 (1979).

36. W. Wang, P. D. Lee, M. McLean, A model of solidification microstructures in nickel-based superalloys: predicting primary dendrite spacing selection. *Acta Materialia* **51**, 2971 (Jun, 2003).

37. S. Vernède, P. Jarry, M. Rappaz, A granular model of equiaxed mushy zones: Formation of a coherent solid and localization of feeding. *Acta Materialia* **54**, 4023 (2006/9, 2006).

38. M. Sistaninia, A. B. Phillion, J. M. Drezet, M. Rappaz, Simulation of Semi-Solid Material Mechanical Behavior Using a Combined Discrete/Finite Element Method. *Metallurgical and Materials Transactions A* **42A**, 239 (Jan, 2011).

39. A. B. Phillion, S. Vernede, M. Rappaz, S. L. Cockcroft, P. D. Lee, Prediction of solidification behaviour via microstructure models based on granular structures. *International Journal of Cast Metals Research* **22**, 240 (Aug, 2009).